

Induced Disassembly of a Virus-like Particle under Physiological Conditions for Venom Peptide Delivery

M. Patrick Kelly, Tanya Napolitano, Prachi Anand, Justin S. K. Ho, Shakeela Jabeen, Jessica Kuppan, Sujoy Manir, and Mandé Holford*



Cite This: *Bioconjugate Chem.* 2021, 32, 111–120



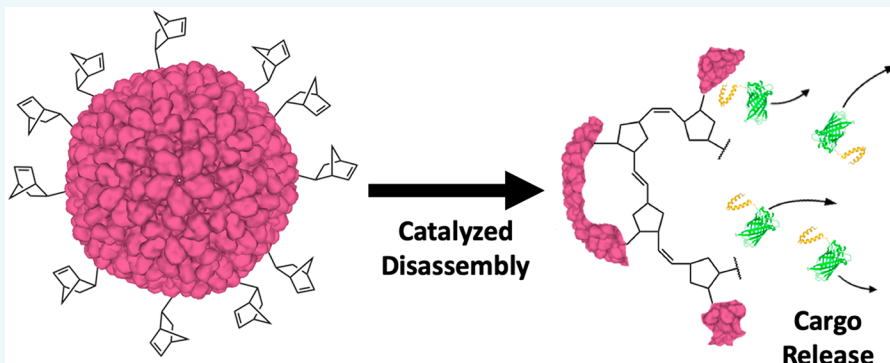
Read Online

ACCESS |

Metrics & More

Article Recommendations

Supporting Information



ABSTRACT: Virus-like particles (VLPs) show considerable promise for the *in vivo* delivery of therapeutic compounds such as bioactive venom peptides. While loading and targeting protocols have been developed for numerous VLP prototypes, induced disassembly under physiological conditions of neutral pH, moderate temperature, and aqueous medium remain a challenge. Here, we implement and evaluate a general mechanism, based on ring-opening metathesis polymerization (ROMP), for controllable VLP disassembly. This mechanism is independent of cell-specific factors or the manipulation of environmental conditions such as pH and temperature that cannot be readily controlled *in vivo*. The ROMP substrate norbornene is covalently conjugated to surface-exposed lysine residues of a P22 bacteriophage-derived VLP, and ROMP is induced by treatment with the water-soluble ruthenium catalyst AquaMet. Disruption of the P22 shell and release of a GFP reporter is confirmed via native agarose electrophoresis, TEM, and dynamic light scattering (DLS) analyses. Our ROMP disassembly strategy does not depend on the particular structure or morphology of the P22 nanocontainer and is adaptable to other VLP prototypes for the potential delivery of venom peptides for pharmacological applications.

INTRODUCTION

Venom peptides, which have evolved to have extremely powerful and narrowly targeted physiological effects, possess immense therapeutic potential for the treatment of various human disease and disorders, including cancer and pain.^{1–3} As of 2018, there were more than 60 U.S. Food and Drug Administration-approved peptide drugs on the market, with hundreds more in various stages of development.^{4–6} Peptides as therapeutics are generally nontoxic, highly potent, and, in most cases, extremely specific, with few side effects.^{7,8} However, the delivery of therapeutic peptides to their molecular targets *in vivo* remains a significant challenge. Only a handful of peptides are robust enough to be administered orally, thus ruling out the most common and least invasive delivery route. Moreover, with the exception of specialized cell-penetrating peptides, very few peptides are able to cross the cell membrane or the blood-brain barrier (BBB).⁹ These hurdles have prevented the widespread development and

application of bioactive peptides. A prominent example of a venom peptide therapeutic that has enormous physiological potential but whose delivery hampers broad application is the drug ziconotide (Prialt), which is derived from venomous cone snail *Conus magus* and used to treat chronic pain in HIV and cancer patients.^{10,11} Ziconotide does not cross the BBB and has to be administered by intrathecal injection. Despite the fact that ziconotide is a nonaddictive analgesic, active on N-type calcium channels and not opioid receptors, its invasive method of delivery restricts its use. There is a pressing need for innovative peptide drug delivery methods that will enable the

Received: September 3, 2020

Revised: October 26, 2020

Published: December 11, 2020



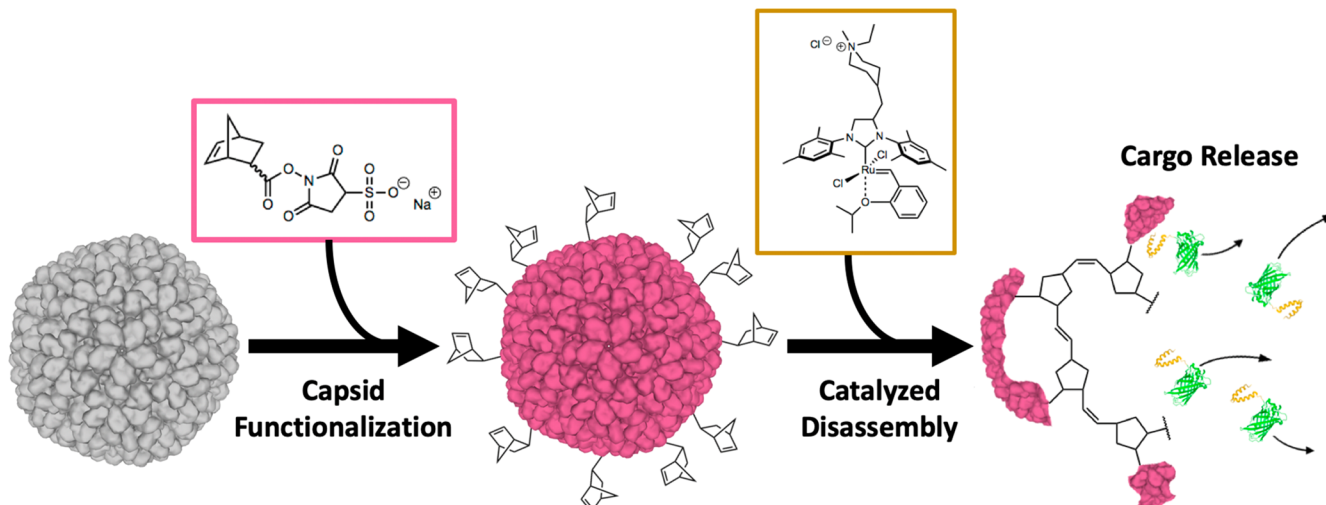


Figure 1. Physiological delivery of therapeutic peptides using functionalized VLP nanocontainers with a triggered disassembly strategy. First, P22-derived VLPs are loaded with an arbitrary protein or peptide cargo. This is accomplished by coexpression of the P22 coat protein with a fusion construct consisting of the cargo of interest (here, GFP, shown in green) and the C terminus of the P22 scaffold protein (gold), which nucleates capsid self-assembly through noncovalent association with the interior of the coat protein shell and then remains in the capsid interior. After purification through standard methods, the loaded VLPs are functionalized by covalent attachment of a ROMP substrate (here, an NHS-activated norbornene-COOH) to surface-exposed lysine residues of the coat protein shell. Finally, functionalized VLPs are disassembled under physiological conditions through the introduction of a ruthenium catalyst and initiation of ring-opening metathesis polymerization (ROMP).

untapped diversity of venom peptides to be utilized for pharmaceutical development.

There are several strategies for improving the pharmacokinetic profile of bioactive peptides. One approach is to stabilize the structure of the peptide itself through such methods as peptide stapling, macrocyclization, or grafting of peptide segments onto a protein scaffold.¹² However, as these methods involve changes in secondary and tertiary structures, they may disturb the function of the peptide.

Another strategy for *in vivo* drug delivery, in particular peptide delivery, is to package the therapeutic agent within a “Trojan Horse”, a macromolecular carrier that can protect the payload in transit and release it upon reaching the site of action. This approach has received significant attention recently for its role as a delivery mechanism for mRNA vaccines. For example, mRNA-1273, Moderna’s candidate vaccine for COVID-19, uses a lipid nanoparticle (LNP) to deliver an mRNA for the SARS-CoV-2 spike protein to cellular ribosomes.^{13–15} Other types of macromolecules have been studied for their potential as carriers as well, including natural and synthetic copolymers, inorganic particles, DNA origami, and noninfectious virus-like particles (VLPs) derived from the protein capsids of viruses.^{16–21} We previously used a VLP Trojan Horse strategy to encapsulate ziconotide and shuttle it across a BBB model to demonstrate the proof-in-principle of venom peptide delivery using viral capsids.^{22,23}

Because viral capsids have specifically evolved to protect viral genomes and deliver them to host cells, VLPs are especially attractive candidates for macromolecular nanocontainers. VLPs can also be produced in large quantities through heterologous expression and precisely manipulated with the tools of protein engineering.²⁴ Systems for the encapsulation of peptides or proteins have been reported for a number of VLP prototypes, including those derived from the cowpea chlorotic mottle virus (CCMV), Hepatitis B core antigen particles (HBVc), and the bacteriophages MS2, Q β , and P22. These systems employ a variety of mechanisms for packaging peptides or proteins, including electrostatic

interactions, passive diffusion, direct conjugation of the cargo to genomic RNA, and construction of a chimeric coat- or scaffold–cargo fusion.^{25–29}

The bacteriophage P22 *Salmonella typhimurium* system used in this report allows for the sequestration of an arbitrary, genetically encoded peptide or protein cargo through the heterologous expression in *E. coli* of (1) the P22 coat protein and (2) a fusion of the cargo of interest with the truncated C terminus of the P22 scaffold protein, which nucleates capsid self-assembly.²⁹ Coexpression of these two gene products leads to self-assembly of P22 VLP nanocontainers loaded with 200–300 copies of the noncovalently bound cargo–scaffold fusion. The VLPs thus produced are highly stable and can be purified through standard methods. This system can produce very high effective local concentrations of the cargo package.³⁰ In addition to our method for translocating P22-derived VLPs containing the neuroactive ziconotide peptide across a BBB mimic, strategies have also been reported for the cleavable release of cytotoxic cargo peptides in response to Cathepsin B, a protease overexpressed in many tumor cells.^{22,23,31} However, the development of a general, as opposed to cell-specific, mechanism for triggered VLP release *in vivo* remains an active area of research.

Here, we implement and evaluate a general mechanism for controllable disassembly that does not rely on either cell-specific factors or the manipulation of environmental conditions such as pH and temperature that cannot be readily controlled *in vivo*.¹² Our strategy for triggered disassembly of the P22 VLP nanocontainer employs the bioorthogonal ring-opening metathesis polymerization (ROMP) reaction, which is known to proceed under physiological conditions in the presence of a ruthenium catalyst (Grubbs Catalyst).^{32,33} Our strategy consists of two steps: First, N-hydroxysuccinimide-activated norbornene moieties are covalently attached to multiple surface-exposed lysine residues on the VLP exterior via standard bioconjugation methods.³⁴ Then, a bioorthogonal ring-opening metathesis polymerization (ROMP) reaction is initiated by the introduction of a water-tolerant ruthenium

catalyst.^{35,36} The resulting ROMP reaction is driven by the release of ring strain in the norbornene substrate to trigger disassembly of the VLP and release of the cargo–scaffold fusion, which is not covalently attached to the disassembled coat-protein chassis (Figure 1).

ROMP, as the name suggests, is a polymerization reaction initiated by a transition metal catalyst and driven by the release of ring strain in a cyclic olefin such as cyclobutene, cyclopentene, cyclooctene, or norbornene.³⁷ The ROMP reaction is a powerful and broadly applicable tool for synthesizing macromolecular substances.³⁸ Its versatility in polymer chemistry has led to the development of well-defined ROMP catalysts with specialized properties, including catalysts with tailored initiation or propagation rates, water-tolerant and water-soluble catalysts, and photoactivated catalysts.^{39–42} The AquaMet catalyst utilized in this report is a variant of the widely available Grubbs II ruthenium catalyst (Figure 2). The

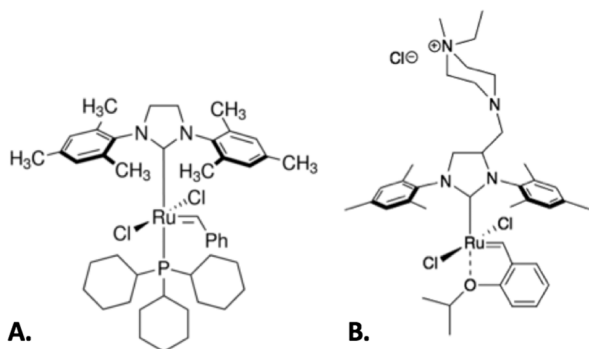


Figure 2. Ruthenium metathesis catalysts used for ROMP disassembly of VLP nanocontainers. The Grubbs II catalyst (A) and the AquaMet catalyst (B). The quaternary ammonium group appended to the N-heterocyclic carbene ligand provides improved solubility in water.

Grubbs catalysts are notable for their water-tolerance, for their effectiveness at low concentrations (as low as 2 mol %), and for the fact that the resulting ROMP reactions unfold on a physiologically relevant time scale (often on the order of minutes). In addition, the AquaMet catalyst incorporates a quaternary ammonium group and is thus highly water-soluble.^{43,44}

In a previous study, we reported pilot results of this Trojan Horse strategy. P22-derived nanocontainers loaded with a GFP cargo (P22_GFP) were recombinantly expressed and purified, and the resulting VLP was functionalized by covalent conjugation of the ROMP substrate norbornene to the capsid surface. Treatment of the functionalized nanocontainers with a second-generation Grubbs catalyst (Grubbs II) resulted in significant morphological distortion with respect to untreated constructs, as indicated by TEM micrographs. However, direct evidence of cargo release was not observed.²³ In the present study, we reexamine the induced disassembly of norbornene-functionalized P22_GFP constructs treated with the water-soluble AquaMet catalyst (Figure 2).⁴⁵ In addition, a cargo-release assay was developed and implemented to monitor the release of the packaged GFP reporter into the solvent phase following catalyst treatment.

RESULTS AND DISCUSSION

To determine the catalyst concentration needed to trigger the ROMP reaction and subsequent disassembly in functionalized capsids, serial dilutions of catalyst were prepared and used to treat aliquots of P22 nanocontainers. To monitor for nonspecific catalyst effects, nonfunctionalized P22 nanocontainers were used as controls. Reactions were incubated overnight at room temperature and characterized by native agarose electrophoresis. The resulting native agarose gels indicate a clear difference in the behavior of nanocontainers conjugated with the ROMP-substrate norbornene (P22His₆GFP_Norb) and nanocontainers that lack the norbornene moiety (P22His₆GFP) (Figure 3A). A nonspecific catalyst effect is observed at high catalyst concentrations (Lane 5); however, functionalized nanocontainers (P22His₆GFP_Norb) appear to dissociate at catalyst concentrations that have no observable effect on nonconjugated nanocontainers (P22His₆GFP_Norb).

We next compared ROMP-induced disassembly with heat-induced disassembly. Past studies have demonstrated that heating P22 VLPs at 65 °C results in capsid expansion, a morphological change that mimics the expansion of capsids during DNA packaging in the natural P22 life cycle. Additional heating at 75 °C induces release of the pentameric subunits from the 5-fold icosahedral vertices, resulting in the so-called “wiffle-ball” conformation and the release of packaged cargo.⁴⁶ To examine the behavior of functionalized capsids under a thermal gradient, we again used native agarose electrophoresis (Figure 3B). As expected, heat-induced disassembly was observed, albeit at a slightly lower temperature (starting at 70 °C) than reported for the case of nonfunctionalized capsids (>80 °C). Importantly, treatment of functionalized P22 constructs with catalyst concentrations above 0.054 mg/mL produced smeared bands (Figure 3A, Lanes 7–10) that resemble those of capsids heated at 65 °C or higher (Figure 3B, Lanes 6–10).

Dynamic light scattering (DLS) confirmed that ROMP functionalization did not significantly alter either the size or the morphology, as measured by the hydrodynamic diameter and polydispersity index (PDI), of P22 nanocontainers. However, DLS analysis of functionalized nanocontainers (P22His₆GFP_Norb) treated with AquaMet catalyst revealed a pronounced, dose-dependent increase in both the mean hydrodynamic diameter and the PDI with increasing catalyst concentration (Figure 4). These results are consistent with ROMP-induced dissociation and/or aggregation.

TEM micrographs of norbornene-conjugated nanocontainers (P22His₆GFP_Norb) treated with AquaMet water-soluble ruthenium catalyst exhibit significant distortion in capsid morphology. Aggregates of what appear to be disrupted and fused capsids are plainly visible. We were unable to locate any of the regular icosahedral structures characteristic of P22 VLP not reacted with the AquaMet catalyst (Figure 5). The observation of disordered aggregates is consistent with a polymerization reaction that occurs at both intra- and inter-nanocontainer interfaces.

To further confirm that P22 ROMP functionalized nanocontainers were undergoing structural disruptions that may indicate disassembly, we developed a cargo release fluorescence assay in which we monitored the release of the His₆-GFP cargo from control (P22 His₆GFP_Norb, no catalyst) and experimental (P22His₆GFP_Norb, 0.212 mg/mL AquaMet

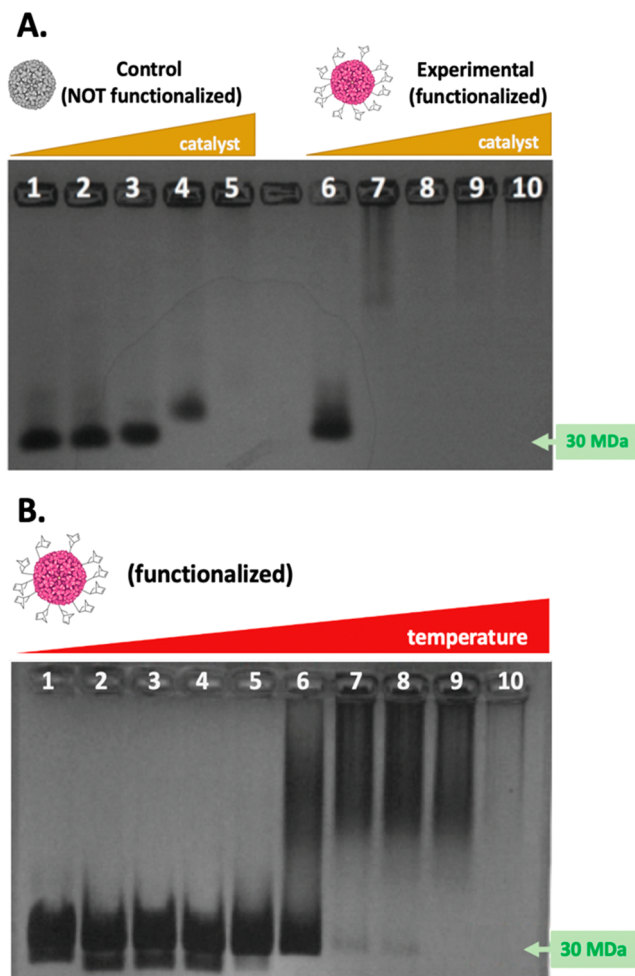


Figure 3. Catalyst-activated disassembly of P22-derived VLP nanocontainers. (A) Treatment of 70 μ L (1.29 mg/mL) aliquots of nonfunctionalized (P22His₆GFP_WT, left) and functionalized (P22His₆GFP_Norb, right) nanocontainers with increasing concentrations (0–0.28 mg/mL, Table S1) of AquaMet catalyst indicates capsid disassembly at significantly lower catalyst concentrations for functionalized nanocontainers illustrate change in structure. While functionalized capsids disassemble at 0.054 mg/mL catalyst (Lane 7), the 30 MDa band corresponding to the fully assembled capsid only disappears at a catalyst concentration of 0.28 mg/mL (Lane 5) for nonfunctionalized capsids. It appears that disassembly or some other phenotypic change is occurring on nonfunctionalized nanoparticles at high dosage of AquaMet. We speculate that it may be due to the action of the catalyst solution on the gel matrix. (B) Heat-activated disassembly of functionalized nanocontainers (P22GFP_Norb). Functionalized nanocontainers (P22_GFP_Norb) were divided into 15 μ L aliquots and heated for 10 min at a temperature gradient of 50–85 °C (Table S2), then subject to native agarose electrophoresis. The onset of disassembly is observed in the 65–70 °C range (lanes 6–7), as indicated by smearing and gradual disappearance of the 30 MDa band visible in the control (Lane 1, no heat). Note that band smearing is also visible in Lanes 7–10 in (A) above.

catalyst) samples. Each of the samples was incubated with Ni²⁺ Sepharose beads, then washed and eluted, as described below. The four wash fractions and four elution fractions were monitored for absorbance at 280 nm (aromatic amino acids λ_{max}) and 495 nm (GFP λ_{max}). A significant peak was observed in the elution fractions of the experimental sample at both wavelengths (Figure 6). No peak was observed in the elution fractions of the control sample. These results demonstrate

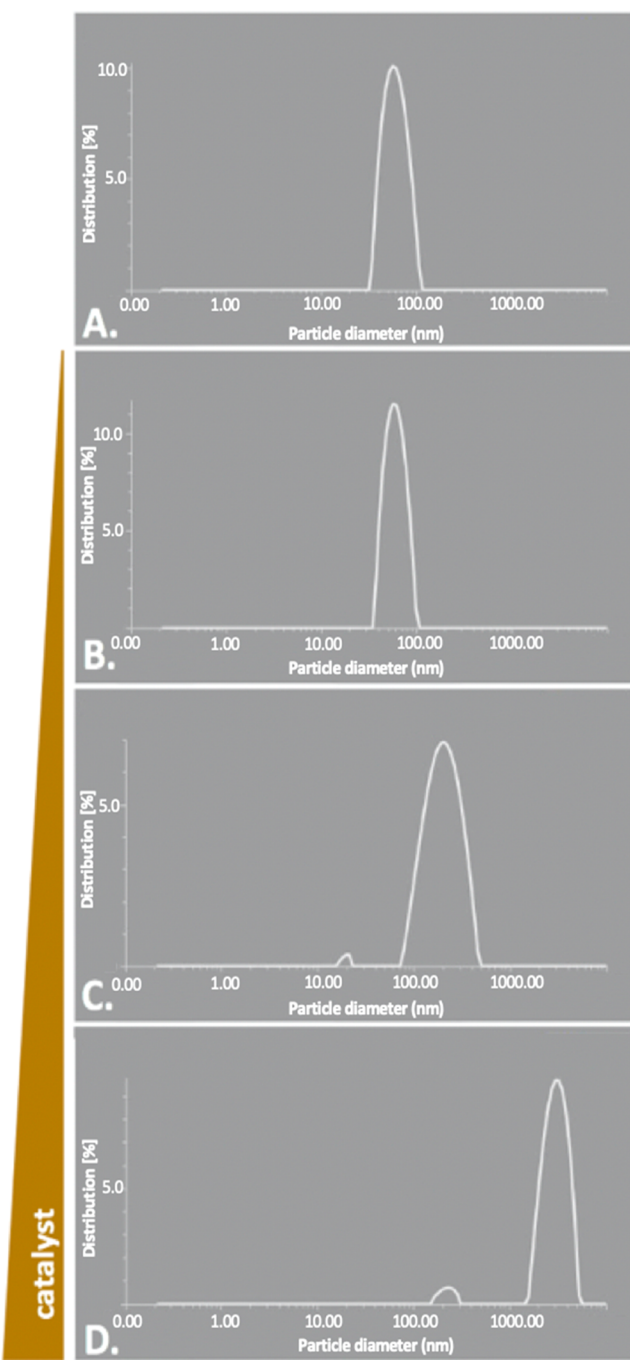


Figure 4. DLS characterization of norbornene conjugated nanocontainers illustrate change in structure. Functionalized nanocontainers (P22His₆GFP_Norb) were divided into 82.5 μ L aliquots (1.09 mg/mL) and treated with increasing concentrations (0–0.325 mg/mL) of catalyst. DLS characterization of the hydrodynamic diameter and polydispersity index (PDI) reveals a steady migration of the size distribution peak toward larger diameters accompanied by an increase in PDI with increasing catalyst concentration. (A) no catalyst, $d_{\text{mean}} = 60.2$ nm, PDI = 15.1%. (B) 13 μ g/mL catalyst, $d_{\text{mean}} = 60.6$ nm, PDI = 7.5%. (C) 130 μ g/mL catalyst, $d_{\text{mean}} = 193.5$ nm, PDI = 21.9%. (D) 325 μ g/mL catalyst, $d_{\text{mean}} = 3222$ nm, PDI = 26.9%.

induced release of the cargo protein at physiological conditions (PBS, 37 °C).

To monitor cytotoxicity of the nonfunctionalized P22His₆GFP and functionalized P22His₆GFP_Norb con-

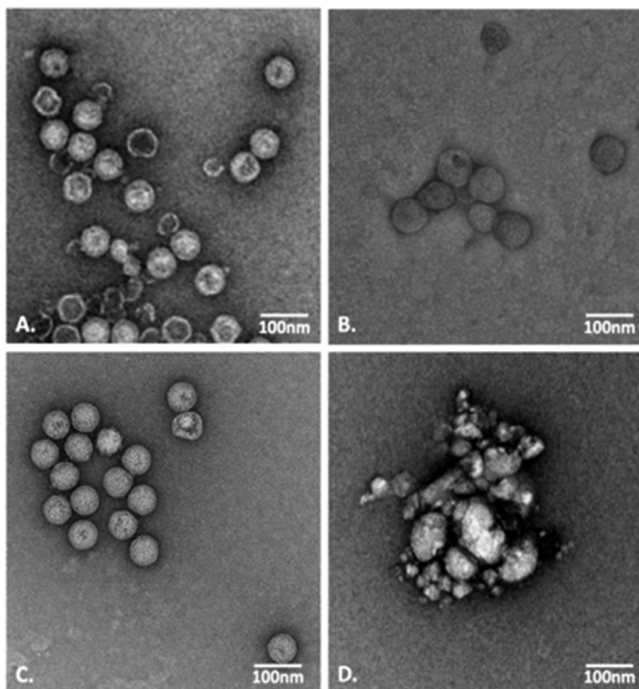


Figure 5. TEM images show phenotypic change suggesting disassembly of P22 capsid. Images show (A) untreated, non-functionalized constructs (P22His₆GFP_WT, no catalyst), (B) untreated, functionalized constructs (P22His₆GFP_Norb, no catalyst), (C) nonfunctionalized constructs treated with AquaMet catalyst (P22His₆GFP_WT, 0.45 mg/mL catalyst), and (D) functionalized constructs treated with AquaMet catalyst (P22His₆GFP_Norb, 0.325 mg/mL catalyst).

structs, MTT assays were conducted using BJ normal foreskin epithelial cells. No evidence of cytotoxicity was found for treatment with VLP constructs at concentrations up to 100 $\mu\text{g}/\text{mL}$ (Figure 7A).

Finally, to assess the cytotoxicity of the AquaMet catalyst, we conducted MTT assays in HeLa and 1MEA cell lines. While moderate cytotoxicity (>10% cytotoxicity, <60% viability) was found for catalyst concentrations above 200 $\mu\text{g}/\text{mL}$ in HeLa cells, this value is significantly higher than the 50–100 $\mu\text{g}/\text{mL}$ needed to disrupt functionalized P22His₆GFP_Norb constructs without affecting nonfunctionalized P22His₆GFP constructs (Figure 7B). As a reference, these catalyst concentrations are roughly comparable to the reported peak serum concentrations of a variety of common drugs, including ibuprofen ($61.1 \pm 5.5 \mu\text{g}/\text{mL}$), aspirin ($24 \pm 4 \mu\text{g}/\text{mL}$), the antiviral cidofovir ($19.6 \pm 7.2 \mu\text{g}/\text{mL}$), and the β -lactam antibiotic cefepime ($65 \pm 7 \mu\text{g}/\text{mL}$).⁴⁷ Finally, no significant cytotoxicity was found for 1MEA cells.

CONCLUSIONS

Native agarose electrophoresis, dynamic light scattering (DLS), and transmission electron microscopy (TEM) all indicate that treatment of ROMP-functionalized P22 nanocontainers with a water-soluble ruthenium catalyst (AquaMet) results in significant disassembly of the P22 constructs. Studies of the physical virology of the P22 bacteriophage confirm that the ROMP reaction induced here provides sufficient energy for disassembly. For example, one study estimated that each of the 420 coat protein monomers contributes -7.2 kcal/mol to procapsid stability, while each of the 200–300 scaffold proteins

Cargo-release from catalyst-treated P22 Constructs

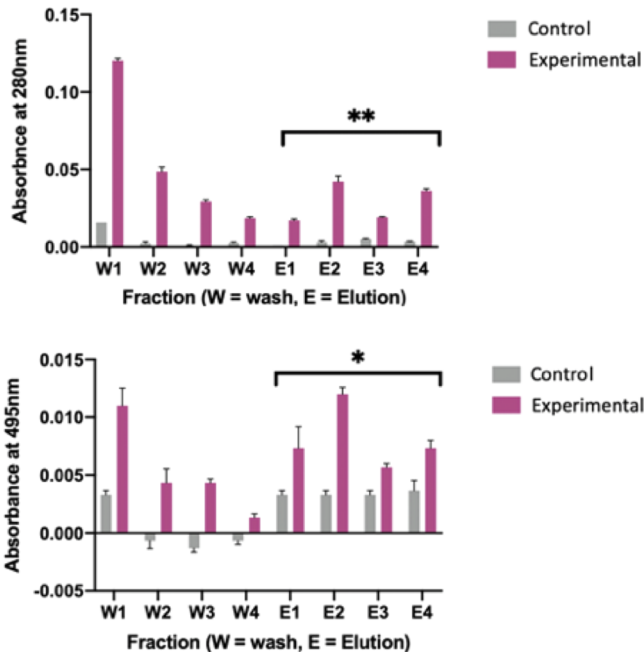


Figure 6. Cargo-release assay indicated induced release of GFP protein at physiological conditions. Functionalized (P22His₆GFP_Norb) constructs were loaded with 200–300 copies of a His-tagged GFP reporter and treated with 0.212 mg/mL AquaMet catalyst (experimental, magenta) or ddH₂O (control, grey). Samples were incubated with Ni²⁺ Sepharose beads, then washed and eluted. Absorbance profiles of experimental constructs exhibit a strong peak at the start of elution (fraction E1) for both 280 and 495 nm (the λ_{max} of GFP) with $p^{**} = 0.066$ at 280 nm and $p^* = 0.0142$ at 495 nm experimental vs control elution fractions, respectively.

contributes -6.1 kcal/mol .⁴⁸ These estimates assume that (1) each scaffold protein contributes the whole of its binding energy to procapsid stability, and (2) all procapsids contain the same number of scaffold proteins.⁴⁹ While these assumptions are not entirely realistic, they provide an upper-bound estimate for the binding energy of the procapsid as a whole: (420 coat proteins)(7.2 kcal/mol) + (300 scaffold proteins)(6.1 kcal/mol) \approx 5000 kcal/mol. As noted above, polymer elongation by ROMP is driven by the release of ring strain in a cyclic olefin substrate. The ring strain of norbornene, the ROMP substrate used here, is 27.2 kcal/mol.⁵⁰ With an average of 4.12 norbornene-functionalized lysines per coat protein monomer, this yields approximately 47,000 kcal/mol ring strain energy per functionalized capsid.⁵¹ Thus, only \sim 10% of the theoretical yield of norbornene ring strain energy needs to be harnessed to reach the disassembly threshold.

We also found significant evidence of cargo release under physiological conditions, as indicated by an increase in absorbance at 280 and 495 nm following capsid disruption. The increase at the 495 nm peak in particular indicates that some of the released cargo was still functional, i.e., the tertiary structure was not significantly altered. To roughly quantify the active GFP released into the solution phase, we assume an average VLP mass of 32.4 MDa and an average loading of 281 EGFP per capsid, as reported for the P22 system by O'Neil et al., and note the extinction coefficient of $\epsilon = 55,000 \text{ cm}^{-1} \text{ M}^{-1}$ for EGFP.^{52,53} These figures indicate that 1–2% of active GFP was released into the solution phase. However, the substantial

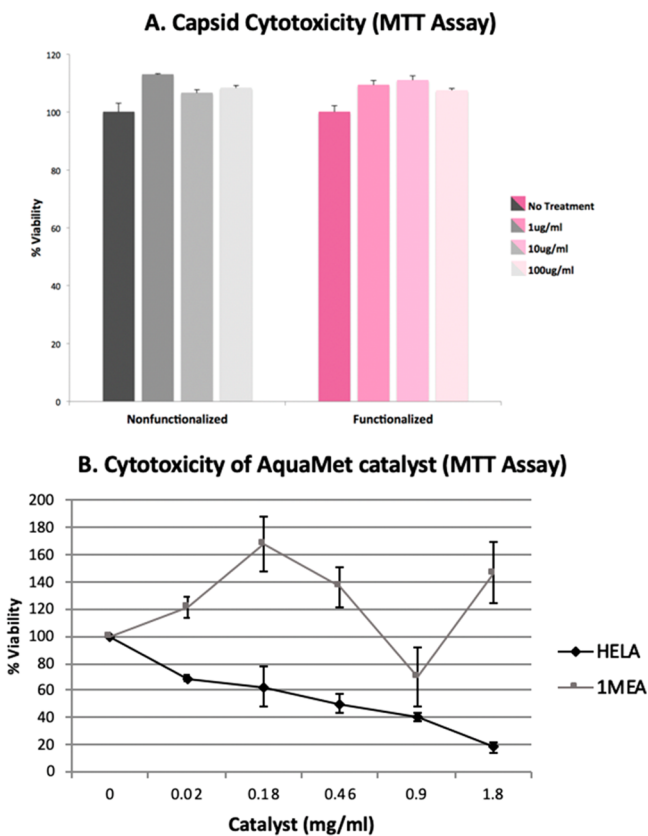


Figure 7. No significant cytotoxicity found of P22 constructs and ruthenium catalysts. (A) Nonfunctionalized P22His₆GFP and functionalized P22His₆GFP_Norb capsids are not cytotoxic. In MTT assays using BJ normal foreskin epithelial cells, neither nonfunctionalized (gray) nor functionalized (magenta) P22 VLP constructs show significant cytotoxicity below 0.1 mg/mL. (B) In MTT assays using 1MEA and HeLa cell lines with varying concentrations of AquaMet catalyst, it was found that the catalyst is moderately cytotoxic in HeLa cells at concentrations above ~0.2 mg/mL which is well above what is required for ROMP reaction to induce disruption in the VLP.

peak at 280 nm, together with the fact that GFP fusions tend not to fold properly, suggests that the total cargo released (including inactive GFP) is significantly higher.⁵⁴

While we previously demonstrated the loading of the venom peptide ziconotide into P22-derived VLPs, a disassembly assay for venom peptide cargoes (as opposed to a GFP cargo) has yet to be developed.²² Because VLP assembly and cargo loading are carried out entirely *in vivo* in the P22 system, we require a peptide labeling method that can likewise be implemented *in vivo*. One approach might be to use noncanonical amino acid mutagenesis (ncAA mutagenesis) to incorporate an engineered amino acid fluorophore, for example, the tryptophan analogue 4-cyanotryptophan, directly into cargo peptide.⁴¹

Finally, we found that the catalyst concentrations needed for capsid disruption are not significantly cytotoxic and are within the effective concentrations of some common pharmaceuticals. VLPs and VLP-derived nanoparticles have been studied extensively in recent years for their biomedical potential, in particular for use in gene therapy and the targeted delivery of therapeutic and diagnostic agents.^{21,55} While gene therapy applications generally use VLPs derived from mammalian viruses, other therapeutic and diagnostic applications tend to

focus on plant viruses and bacteriophages, which are less likely to trigger pathogenic virus–host interactions.⁵⁶ One recent study found no evidence of overt toxicity in naive and immunized mice after single injections of protein cages derived from the Cowpea Chlorotic Mottle Virus (CCMV) and the heat shock protein cage (Hsp). Both CCMV and Hsp exhibited broad distribution throughout most tissues and organs, and were rapidly excreted, with no evidence of long-term persistence. While these findings suggest that P22-derived nanocontainers may be safe for biomedical applications, a comprehensive study has yet to be conducted.⁵⁷

While the potential toxicity of the transition metal olefin catalysts has not been well researched, there are some indications that ruthenium (Ru) is genotoxic.⁵⁸ Our results for cytotoxicity were mixed, and suggested that results will vary depending on the cell line used. Future efforts will include an increase in variety of both disease and normal cell lines in order to obtain a more accurate account of catalyst toxicity in human cell lines. These concerns are offset by the fact that very small quantities of ruthenium generally suffice to catalyze ROMP.⁵⁹ While other transition metals, including tungsten, molybdenum, titanium, and tantalum, have been found to catalyze olefin metathesis, catalysts based on these elements generally either cross-react with or are inhibited by other functionalities, which reduces their utility in biological contexts, particularly in aqueous media.^{60,61}

An additional concern with this system pertains to the toxicity and *in vivo* persistence of the polynorbornene backbone produced by ROMP disassembly. Several studies have demonstrated that polynorbornenes are not cytotoxic.^{62–64} However, because these macromolecules feature an all-carbon backbone, they are not readily degradable. Nevertheless, recent work has shown that doping the pool of norbornene ROMP precursors with silyl ether-based cyclic olefins results in degradable backbones with significantly improved long-term clearance profiles.⁶⁵ This suggests a promising avenue for future study.

In contrast to other VLP delivery systems, which rely on passive diffusion or environmental conditions such as hydrophobicity,⁶⁶ pH (typically through the endosomal pathway), and cell-specific proteases³¹ for cargo release, the system described here employs a bioorthogonal ROMP reaction. Importantly, the ROMP delivery system is modular: First, the protein cargo is genetically encoded, and thus arbitrary. Further, the functionalization method (bioconjugation via an activated NHS-ester) and trigger protocol (treatment with a water-soluble ruthenium catalyst) are completely general, and expected to translate to other VLP systems, whether derived from other phage particles or wholly synthetic. Finally, the ROMP reaction itself is bioorthogonal, and is thus independent of environmental conditions and cell-specific factors.

While surface-exposed lysine residues were used as functionalization handles in this report, selective bioconjugation is also possible on cysteine, tyrosine, and methionine residues.⁶⁷ Future efforts might thus focus on the construction of bifunctional VLPs decorated with targeting molecules such as cell-penetrating peptides or antibody fragments in addition to ROMP substrates. We envision a wholly modular peptide drug delivery system that combines a genetically programmed cargo with an arbitrary targeting moiety and an interchangeable VLP chassis. Because both VLP constructs and catalyst are water-soluble, we envisage a two-stage delivery process via

intravenous drip therapy, similar to saline. First, VLPs loaded with the peptide of interest and functionalized with a ROMP substrate in addition to a targeting moiety such as HIV-Tat (as demonstrated in our previous report²²), could be administered and allowed to localized at the target. After sufficient time for the clearance of nonlocalized VLPs, administration of the bioorthogonal catalyst solution would trigger the release of cargo at the target site (and only at the target site). Such a delivery system could significantly advance the use of venom peptides for therapeutic development.

■ EXPERIMENTAL PROCEDURES

Construction of P22His₆GFP Nanocontainers. A Q5 site-directed mutagenesis kit (New England Biolabs) was used to insert a hexahistidine tag at the N-terminal of the SP141-GFP gene of the P22GFP expression plasmid via standard PCR protocols. Transformed clones were screened for correct insertion of the hexahistidine tag and confirmed by Sanger sequencing (Genewiz, Figure S1). P22His₆GFP nanocontainers were expressed and purified as described in O’Neil et al. Briefly, BL21(DE3) *E. coli* were transformed with the P22His₆GFP expression plasmid, grown to an OD₆₀₀ = 0.6 in LB medium and induced with isopropyl β-D-1-thiogalactopyranoside (IPTG, 1 mM). After 4 h, cells were harvested, lysed by treatment with DNase, RNase, and lysozyme, and then sonicated. The clarified lysate was ultracentrifuged over a 35% (w/v) sucrose cushion, dialyzed against pH 7.2 PBS overnight, then concentrated and resuspended in pH 7.2 PBS using a 100 kDa MWCO centrifugal filter device (Amplicon). Expression and self-assembly of P22 VLPs was confirmed by native agarose electrophoresis (Figure 3A) and ESI-MS (Figure S5).

Conjugation of Norbornene to P22His₆GFP VLPs. To conjugate norbornene to surface-exposed lysine residues on the P22 bacteriophage capsid, 19.2 mg (1 × 10⁻⁴ mol) of 1-ethyl-3-(3-(dimethylamino)propyl) carbodiimide (EDC) and 21.2 mg (1 × 10⁻⁴ mol) *N*-hydroxysuccinimide (sulfo-NHS) were added to 1 mL of a 0.1 M solution of 5-norbornene-2-carboxylic acid in 0.1 M phosphate buffer (pH 6.0) (all reagents purchased from Sigma-Aldrich). The solution was allowed to react at room temperature with intermittent vortexing. After 30 min, 180 μL of the sulfo-NHS/EDC/Norbornene solution was added to 1 mL of P22His₆GFP (5 mg/mL) in PBS (pH 7.6). After reacting at room temperature overnight on a shaker at 250 rpm, the product was concentrated by means of a 100 kDa MWCO centrifugal filter device (Amplicon) and resuspended in pH 7.2 phosphate buffer. Conjugation of norbornene-COOH to the P22 coat protein was confirmed by ESI-MS (Figure S6).

DLS Characterization of P22His₆GFP Nanocontainers. P22His₆GFP nanocontainers at a concentration of 10 μM in pH 7.2 PBS were filtered through a 0.2 μm syringe filter and transferred to a low-volume (45 μL) quartz cuvette for DLS analysis with an Antor Paar Litesizer 500 instrument. All data were analyzed using the Kalliope software package.

Native Agarose Electrophoresis. All P22His₆GFP_Norb samples were normalized with respect to protein concentration prior to native agarose electrophoresis. A 20 μL aliquot was removed from each sample, mixed with loading buffer (40% glycerol, bromophenol blue) and loaded into the wells of a 1.0% native agarose gel. Gels were run at 65 V for 2.5 h in TBE buffer (89 mM Tris, 89 mM borate, 2 mM EDTA), and then stained with Coomassie blue and de-stained with acetic acid

and methanol. Images were produced using a Foto/Analyst FX imaging system (Fotodyne).

Cargo-Release Disassembly Assay. 250 μL aliquots of a 2.5 mg/mL solution of P22His₆GFP_Norb in PBS were placed in each of two microcentrifuge tubes. To the experimental sample was added 67.3 μL of a 1 mg/mL solution of AquaMet catalyst in ddH₂O (final concentration 212 μg/mL). To the control sample was added 67.3 μL of ddH₂O. Samples were incubated at 37 °C overnight, then supplemented with 250 μL wash buffer (Tris-HCl (10 mM), imidazole (20 mM), NaCl (200 mM), pH 8) and 50 μL Ni²⁺ Sepharose beads and placed on a nutator. After 1 h, the beads were collected by centrifugation (1000g, 1 m) and the flowthrough removed. Beads were resuspended four times in 100 μL of wash buffer, and then eluted four times with 100 μL wash buffer supplemented with 200 mM imidazole. Wash and elution fractions were monitored for absorbance at 280 and 495 nm (peak absorbance of GFP) on a NanoDrop 2000c spectrophotometer (Thermo Scientific).

MTT Cytotoxicity Assay: VLP Constructs. The cytotoxicity of VLPs was examined in BJ normal human foreskin epithelial fibroblasts by MTT assay. 5000 cells were seeded in each well of a 96-well plate and incubated with P22His₆GFP and P22His₆GFP_Norb in quadruplicate at three concentrations: 1 μg/mL, 10 μg/mL, and 100 μg/mL. After 24 h incubation, 20 μL of MTT solution (5.0 mg/mL methyl tetrazolium salt in PBS) was added to each well and plates were incubated for an additional 3 h at 37 °C in 5% CO₂. After 3 h, medium supplemented with MTT solution was aspirated and 100 μL of acidified isopropanol was added to each well. Spectrophotometric assays were conducted in a PowerWave HT Microplate Spectrophotometer at 550 and 620 nm. The mean and standard deviation of the δOD values were calculated by subtracting the 620 nm values from the 550 nm values. The absorbance of control cells (untreated) was used as the 100% viability baseline.

MTT Cytotoxicity Assay: ROMP Catalyst. The cytotoxicity of AquaMet catalyst was examined in HeLa and 1MEA cells by MTT assay, as described above. The cell line BNL1MEA.7R.1, also called 1MEA (mouse liver carcinoma), was a kind gift from Professor Olorenceun Ogunwobi (Hunter College, New York, NY). Cells were maintained in Dulbecco’s modified Eagle’s medium (DMEM, Gibco-BRL Life Technologies, Paisley, UK) supplemented with 10% fetal bovine serum (FBS), 1% penicillin, 4.5 g/L glucose, L-glutamine, and sodium pyruvate. HeLa (human cervical cancer, American Type Culture Collection, Rockville, MD) were regularly cultured in Eagle’s minimal essential medium (Gibco Co., Grand Island, NY) supplemented with 10% fetal bovine serum (FBS), 1% penicillin.⁶⁸

■ ASSOCIATED CONTENT

Supporting Information

The Supporting Information is available free of charge at <https://pubs.acs.org/doi/10.1021/acs.bioconjchem.0c00494>.

DNA sequence of P22 scaffold-GFP fusion protein; DNA sequence of P22 coat protein (P22 CP); protein sequence of P22 scaffold-GFP fusion protein; protein sequence of P22 coat protein; ESI-MS spectrum of P22 coat protein (nonfunctionalized control); conjugation of norbornene-COOH to P22 coat protein ESI-MS data; plasmid map of P22_His₆GFPSPCP construct (PDF);

catalyst concentrations for treatment of nonfunctionalized and functionalized nanocontainers; heat-activated disassembly of functionalized nanocontainers

AUTHOR INFORMATION

Corresponding Author

Mandé Holford – Department of Chemistry and Biochemistry, Hunter College, New York 10065, United States; The Ph.D. Programs in Biochemistry, Chemistry and Biology Graduate Center of the City University of New York, New York 10016, United States; Department of Invertebrate Zoology, The American Museum of Natural History, New York 10024, United States; Department of Biochemistry, Weill Cornell Medicine, New York 10021, United States;
Email: mholford@hunter.cuny.edu

Authors

M. Patrick Kelly – Department of Chemistry and Biochemistry, Hunter College, New York 10065, United States; The Ph.D. Programs in Biochemistry, Chemistry and Biology Graduate Center of the City University of New York, New York 10016, United States; orcid.org/0000-0003-0172-6746

Tanya Napolitano – Department of Chemistry and Biochemistry, Hunter College, New York 10065, United States; The Ph.D. Programs in Biochemistry, Chemistry and Biology Graduate Center of the City University of New York, New York 10016, United States

Prachi Anand – Department of Chemistry and Biochemistry, Hunter College, New York 10065, United States

Justin S. K. Ho – Department of Chemistry and Biochemistry, Hunter College, New York 10065, United States

Shakeela Jabeen – Department of Chemistry and Biochemistry, Hunter College, New York 10065, United States; The Ph.D. Programs in Biochemistry, Chemistry and Biology Graduate Center of the City University of New York, New York 10016, United States

Jessica Kuppan – Department of Chemistry and Biochemistry, Hunter College, New York 10065, United States

Sujoy Manir – Department of Chemistry and Biochemistry, Hunter College, New York 10065, United States

Complete contact information is available at:

<https://pubs.acs.org/10.1021/acs.bioconjchem.0c00494>

Author Contributions

Conceptualization, M.H.; Methodology and Data Analysis, all authors; Writing, P.K., T.N., and M.H.; Project Administration, M.H.; Funding Acquisition, M.H.

Funding

M.H. acknowledges research grants by the Camille & Henry Dreyfus Foundation and the National Institutes of Health (NIH-NIMHD grant 8-G-12-MD007599). M.P.K., T.N., and S.J. acknowledge support from the CUNY Graduate Center Graduate Fellowship program. M.P.K. also acknowledges support from NSF-IGERT to Hunter College. Jessica Kuppan acknowledges support from the NIH-MARC program under award number T34GM007823.

Notes

The authors declare no competing financial interest.

ABBREVIATIONS

VLP, virus-like particle; ROMP, ring-opening metathesis polymerization; P22, Bacteriophage P22; CP, P22 coat protein; SP, P22 scaffold protein; GFP, green fluorescent protein; BBB, blood-brain barrier; DLS, dynamic light scattering; TEM, transmission electron microscopy; PDI, polydispersity index

REFERENCES

- (1) Vetter, I., and Lewis, R. J. (2012) Therapeutic Potential of Cone Snail Venom Peptides (Conopeptides). *Curr. Top. Med. Chem.* 12 (14), 1546–1552.
- (2) Netirojanakul, C., and Miranda, L. P. (2017) Progress and Challenges in the Optimization of Toxin Peptides for Development as Pain Therapeutics. *Curr. Opin. Chem. Biol.* 38, 70–79.
- (3) Akcan, M., Stroud, M. R., Hansen, S. J., Clark, R. J., Daly, N. L., Craik, D. J., and Olson, J. M. (2011) Chemical Re-Engineering of Chlorotoxin Improves Bioconjugation Properties for Tumor Imaging and Targeted Therapy. *J. Med. Chem.* 54 (3), 782–787.
- (4) Lau, J. L., and Dunn, M. K. (2018) Therapeutic Peptides: Historical Perspectives, Current Development Trends, and Future Directions. *Bioorg. Med. Chem.* 26 (10), 2700–2707.
- (5) Napolitano, T., and Holford, M. (2019) Breakthroughs in Venom Peptide Screening Methods to Advance Future Drug Discovery. *Protein Pept. Lett.* 25 (12), 1137–1148.
- (6) Angell, Y., Holford, M., and Moos, W. H. (2019) Building on Success: A Bright Future for Peptide Therapeutics. *Protein Pept. Lett.* 25, 1044.
- (7) Uhlig, T., Kyriyanou, T., Giancarlo, F., Alberto, C., Heiligers, D., Hills, D., Ribes, X., and Verhaert, P. (2014) The Emergence of Peptides in the Pharmaceutical Business: From Exploration to Exploitation. *EuPa Open Proteomics* 4, 58–69.
- (8) Fosgerau, K., and Hoffmann, T. (2015) Peptide Therapeutics: Current Status and Future Directions. *Drug Discovery Today* 20 (1), 122–128.
- (9) Abbott, N. J., Patabendige, A. A. K., Dolman, D. E. M., Yusof, S. R., and Begley, D. J. (2010) Structure and Function of the Blood-Brain Barrier. *Neurobiol. Dis.* 37 (1), 13–25.
- (10) Miljanich, G. (2004) Ziconotide: Neuronal Calcium Channel Blocker for Treating Severe Chronic Pain. *Curr. Med. Chem.* 11 (23), 3029–3040.
- (11) Atanassoff, P. G., Hartmannsgruber, M. W. B., Thrasher, J., Wermeling, D., Longton, W., Gaeta, R., Singh, T., Mayo, M., McGuire, D., and Luther, R. L. (2000) Ziconotide, a New N-Type Calcium Channel Blocker, Administered Intrathecally for Acute Postoperative Pain. *Reg. Anesth. Pain Med.* 25, 274–278.
- (12) Tsomaia, N. (2015) Peptide Therapeutics: Targeting the Undruggable Space. *Eur. J. Med. Chem.* 94, 459–470.
- (13) Kowalski, P. S., Rudra, A., Miao, L., and Anderson, D. G. (2019) Delivering the Messenger: Advances in Technologies for Therapeutic mRNA Delivery. *Mol. Ther.* 27 (4), 710–728.
- (14) Hassett, K. J., Benenato, K. E., Jacquinet, E., Lee, A., Woods, A., Yuzhakov, O., Himansu, S., Deterling, J., Geilich, B. M., Ketova, T., et al. (2019) Optimization of Lipid Nanoparticles for Intramuscular Administration of mRNA Vaccines. *Mol. Ther.-Nucleic Acids* 15 (April), 1–11.
- (15) Thanh Le, T., Andreadakis, Z., Kumar, A., Gómez Román, R., Tolleson, S., Saville, M., and Mayhew, S. (2020) The COVID-19 Vaccine Development Landscape. *Nat. Rev. Drug Discovery* 19 (5), 305–306.
- (16) Lian, T., and Ho, R. J. (2001) Trends and Developments in Liposome Drug Delivery Systems. *J. Pharm. Sci.* 90 (6), 667–680.
- (17) Fleige, E., Quadir, M. A., and Haag, R. (2012) Stimuli-Responsive Polymeric Nanocarriers for the Controlled Transport of Active Compounds: Concepts and Applications. *Adv. Drug Delivery Rev.* 64 (9), 866–884.
- (18) Liang, M., Lu, J., Kovochich, M., Xia, T., Ruehm, S. G., Nel, A. E., Tamanoi, F., and Zink, J. I. (2008) Multifunctional Inorganic

- Nanoparticles for Imaging, Targeting, and Drug Delivery. *ACS Nano* 2 (5), 889–896.
- (19) Huo, M., Yuan, J., Tao, L., and Wei, Y. (2014) Redox-Responsive Polymers for Drug Delivery: From Molecular Design to Applications. *Polym. Chem.* 5 (5), 1519–1528.
- (20) Douglas, S. M., Bachelet, I., and Church, G. M. (2012) A Logic-Gated Nanorobot for Targeted Transport of Molecular Payloads. *Science (Washington, DC, U. S.)* 335 (6070), 831–834.
- (21) Rohovie, M. J., Nagasawa, M., and Swartz, J. R. (2017) Virus-like Particles: Next-Generation Nanoparticles for Targeted Therapeutic Delivery. *Bioeng. Transl. Med.* 2 (1), 43–57.
- (22) Anand, P., O’Neil, A., Lin, E., Douglas, T., and Holford, M. (2015) Tailored Delivery of Analgesic Ziconotide across a Blood Brain Barrier Model Using Viral Nanocontainers. *Sci. Rep.* 5, 12497.
- (23) Kelly, P., Anand, P., Uvaydov, A., and Chakravartula, S. (2015) Developing a Dissociative Nanocontainer for Peptide Drug Delivery. *Int. J. Environ. Res. Public Health* 12, 12543–12555.
- (24) Johnson, J. E. (2010) Virus Particle Maturation: Insights into Elegantly Programmed Nanomachines. *Curr. Opin. Struct. Biol.* 20 (2), 210–216.
- (25) Lee, K. W., Tey, B. T., Ho, K. L., and Tan, W. S. (2012) Delivery of Chimeric Hepatitis B Core Particles into Liver Cells. *J. Appl. Microbiol.* 112 (1), 119–131.
- (26) Van Eldijk, M. B., Wang, J. C. Y., Minten, I. J., Li, C., Zlotnick, A., Nolte, R. J. M., Cornelissen, J. J. L. M., and Van Hest, J. C. M. (2012) Designing Two Self-Assembly Mechanisms into One Viral Capsid Protein. *J. Am. Chem. Soc.* 134 (45), 18506–18509.
- (27) Fiedler, J. D., Brown, S. D., Lau, J. L., and Finn, M. G. (2010) RNA-Directed Packaging of Enzymes within Virus-like Particles. *Angew. Chem., Int. Ed.* 49 (50), 9648–9651.
- (28) Glasgow, J. E., Capehart, S. L., Francis, M. B., and Tullman-Ercek, D. (2012) Osmolyte-Mediated Encapsulation of Proteins inside MS2 Viral Capsids. *ACS Nano* 6 (10), 8658–8664.
- (29) O’Neil, A., Reichhardt, C., Johnson, B., Prevelige, P. E., and Douglas, T. (2011) Genetically Programmed in Vivo Packaging of Protein Cargo and Its Controlled Release from Bacteriophage P22. *Angew. Chem., Int. Ed.* 50 (32), 7425–7428.
- (30) Patterson, D. P., Prevelige, P. E., and Douglas, T. (2012) Nanoreactors by Programmed Enzyme Encapsulation Inside the Capsid of the Bacteriophage P22. *ACS Nano* 6 (6), 5000–5009.
- (31) Wang, J., Fang, T., Li, M., Zhang, W., Zhang, Z. P., Zhang, X. E., and Li, F. (2018) Intracellular Delivery of Peptide Drugs Using Viral Nanoparticles of Bacteriophage P22: Covalent Loading and Cleavable Release. *J. Mater. Chem. B* 6 (22), 3716–3726.
- (32) Binder, J. B., and Raines, R. T. (2008) Olefin Metathesis for Chemical Biology. *Curr. Opin. Chem. Biol.* 12 (6), 767–773.
- (33) Brendgen, T., Fahlbusch, T., Frank, M., Schühle, D. T., Seßler, M., and Schatz, J. (2009) Metathesis in Pure Water Mediated by Supramolecular Additives. *Adv. Synth. Catal.* 351 (3), 303–307.
- (34) Hermanson, G. T. *Bioconjugate Techniques*.
- (35) Binder, J. B., and Raines, R. T. (2008) Olefin Metathesis for Chemical Biology. *Curr. Opin. Chem. Biol.* 12 (6), 767–773.
- (36) Hoveyda, A. H., and Zhugralin, A. R. (2007) The Remarkable Metal-Catalysed Olefin Metathesis Reaction. *Nature* 450 (7167), 243–251.
- (37) Sutthasupa, S., Shiotsuki, M., and Sanda, F. (2010) Recent Advances in Ring-Opening Metathesis Polymerization, and Application to Synthesis of Functional Materials. *Polym. J.* 42 (12), 905–915.
- (38) Bielawski, C. W., and Grubbs, R. H. (2007) Living Ring-Opening Metathesis Polymerization. *Prog. Polym. Sci.* 32 (1), 1–29.
- (39) Ben-Asuly, A., Aharoni, A., Diesendruck, C. E., Vidavsky, Y., Goldberg, I., Straub, B. F., and Lemcoff, N. G. (2009) Photoactivation of Ruthenium Olefin Metathesis Initiators. *Organometallics* 28 (16), 4652–4655.
- (40) Szczepaniak, G., Kosiński, K., and Grela, K. (2014) Towards “Cleaner” Olefin Metathesis: Tailoring the NHC Ligand of Second Generation Ruthenium Catalysts to Afford Auxiliary Traits. *Green Chem.* 16 (10), 4474–4492.
- (41) Schrodi, Y., and Pederson, R. L. *Evolution and Applications of Second-Generation Ruthenium Olefin Metathesis Catalysts*, pp 45–52.
- (42) Ogbu, O. M., Warner, N. C., O’Leary, D. J., and Grubbs, R. H. (2018) Recent Advances in Ruthenium-Based Olefin Metathesis. *Chem. Soc. Rev.* 47 (12), 4510–4544.
- (43) Hong, S. H., and Grubbs, R. H. (2006) Highly Active Water-Soluble Olefin Metathesis Catalyst. *J. Am. Chem. Soc.* 128 (11), 3508–3509.
- (44) Skowerski, K., Szczepaniak, G., Wierzbicka, C., Gulajski, Ł., Bieniek, M., and Grela, K. (2012) Highly Active Catalysts for Olefin Metathesis in Water. *Catal. Sci. Technol.* 2 (12), 2424–2427.
- (45) Skowerski, K., Szczepaniak, G., Wierzbicka, C., Gulajski, Ł., Bieniek, M., and Grela, K. (2012) Highly Active Catalysts for Olefin Metathesis in Water. *Catal. Sci. Technol.* 2, 2424.
- (46) McCoy, K., Selivanovitch, E., Luque, D., Lee, B., Edwards, E., Castón, J. R., and Douglas, T. (2018) Cargo Retention inside P22 Virus-Like Particles. *Biomacromolecules* 19 (9), 3738–3746.
- (47) Goodman, L. S., Brunton, L. L., Chabner, B., and Knollmann, B. C. (2011) *Goodman & Gilman’s Pharmacological Basis of Therapeutics*, 12th ed., McGraw-Hill, New York, NY.
- (48) Parent, K. N., Zlotnick, A., and Teschke, C. M. (2006) Quantitative Analysis of Multi-Component Spherical Virus Assembly: Scaffolding Protein Contributes to the Global Stability of Phage P22 Procapids. *J. Mol. Biol.* 359 (4), 1097–1106.
- (49) Zlotnick, A., Suhanova, M. M., and Teschke, C. M. (2012) The Energetic Contributions of Scaffolding and Coat Proteins to the Assembly of Bacteriophage Procapids. *Virology* 428 (1), 64–69.
- (50) Walker, R., Conrad, R. M., and Grubbs, R. H. (2009) The Living ROMP of Trans-Cyclooctene. *Macromolecules* 42 (3), 599–605.
- (51) Kelly, P., Anand, P., Uvaydov, A., Chakravartula, S., Sherpa, C., Pires, E., O’Neil, A., Douglas, T., and Holford, M. (2015) Developing a Dissociative Nanocontainer for Peptide Drug Delivery. *Int. J. Environ. Res. Public Health* 12 (10), 12543–12555.
- (52) O’Neil, A., Reichhardt, C., Johnson, B., Prevelige, P. E., and Douglas, T. (2011) Genetically Programmed in Vivo Packaging of Protein Cargo and Its Controlled Release from Bacteriophage P22. *Angew. Chem., Int. Ed.* 50 (32), 7425–7428.
- (53) McRae, S. R., Brown, C. L., and Bushell, G. R. (2005) Rapid Purification of EGFP, EYFP, and ECFP with High Yield and Purity. *Protein Expression Purif.* 41 (1), 121–127.
- (54) Pédelacq, J. D., Cabantous, S., Tran, T., Terwilliger, T. C., and Waldo, G. S. (2006) Engineering and Characterization of a Superfolder Green Fluorescent Protein. *Nat. Biotechnol.* 24 (1), 79–88.
- (55) Manchester, M., and Singh, P. (2006) Virus-Based Nanoparticles (VNPs): Platform Technologies for Diagnostic Imaging. *Adv. Drug Delivery Rev.* 58 (14), 1505–1522.
- (56) Koudelka, K. J., Pitek, A. S., Manchester, M., and Steinmetz, N. F. (2015) Virus-Based Nanoparticles as Versatile Nanomachines. *Annu. Rev. Virol.* 2 (1), 379–401.
- (57) Kaiser, C. R., Flenniken, M. L., Gillitzer, E., Harmsen, A. L., Harmsen, A. G., Jutila, M. A., Douglas, T., and Young, M. J. (2007) Biodistribution Studies of Protein Cage Nanoparticles Demonstrate Broad Tissue Distribution and Rapid Clearance in Vivo. *Int. J. Nanomedicine* 2 (4), 715–733.
- (58) Gagnon, Z. E., Newkirk, C., and Hicks, S. (2006) Impact of Platinum Group Metals on the Environment: A Toxicological, Genotoxic and Analytical Chemistry Study. *J. Environ. Sci. Health, Part A: Toxic/Hazard. Subst. Environ. Eng.* 41 (3), 397–414.
- (59) France, M. B., and Uffelman, E. S. (1999) Ring-Opening Metathesis with a Well-Defined Ruthenium Carbene Complex An Experiment for the Undergraduate Inorganic or Polymer Laboratory. *J. Chem. Educ.* 76 (May), 661–665.
- (60) Trnka, T. M., and Grubbs, R. H. (2001) The Development of L₂ × 2 RudCHR Olefin Metathesis Catalysts: An Organometallic Success Story. *Acc. Chem. Res.* 34 (1), 18–29.

- (61) Schrock, R. R., and Hoveyda, A. H. (2003) Molybdenum and Tungsten Imido Alkylidene Complexes as Efficient Olefin-Metathesis Catalysts. *Angew. Chem., Int. Ed.* 42 (38), 4592–4633.
- (62) He, H., Song, B., Qiu, G., Wang, W., and Gu, H. (2020) Synthesis, Conjugating Capacity and Biocompatibility Evaluation of a Novel Amphiphilic Polynorbornene. *Des. Monomers Polym.* 23 (1), 141–154.
- (63) Gonzalez-Fajardo, L., Mahajan, L. H., Ndaya, D., Hargrove, D., Manautou, J. E., Liang, B. T., Chen, M. H., Kasi, R. M., and Lu, X. (2016) Reduced in Vivo Toxicity of Doxorubicin by Encapsulation in Cholesterol-Containing Self-Assembled Nanoparticles. *Pharmacol. Res.* 107, 93–101.
- (64) Patel, P. R., Kiser, R. C., Lu, Y. Y., Fong, E., Ho, W. C., Tirrell, D. A., and Grubbs, R. H. (2012) Synthesis and Cell Adhesive Properties of Linear and Cyclic RGD Functionalized Polynorbornene Thin Films. *Biomacromolecules* 13 (8), 2546–2553.
- (65) Shieh, P., Nguyen, H. V. T., and Johnson, J. A. (2019) Tailored Silyl Ether Monomers Enable Backbone-Degradable Polynorbornene-Based Linear, Bottlebrush and Star Copolymers through ROMP. *Nat. Chem.* 11 (12), 1124–1132.
- (66) Lu, H., Wang, J., Wang, T., Zhong, J., Bao, Y., and Hao, H. (2016) Recent Progress on Nanostructures for Drug Delivery Applications. *J. Nanomater.* 2016, 1.
- (67) Taylor, M. T., Nelson, J. E., Suero, M. G., and Gaunt, M. J. (2018) A Protein Functionalization Platform Based on Selective Reactions at Methionine Residues. *Nature* 562 (7728), 563–568.
- (68) Anand, P., Filipenko, P., Huaman, J., Lyudmer, M., Hossain, M., Santamaria, C., Huang, K., Ogunwobi, O., and Holford, M. Antitumor Effects of Tv1 Venom Peptide in Liver Cancer. *bioRxiv*, 2019. .